ACS OMEGA

Open Access

http://pubs.acs.org/journal/acsodf

Article

Deciphering the Role of H-Ferritin Nanocages in Improving Tumor-Targeted Delivery of Indocyanine Green: Combined Analysis of Murine Tissue Homogenates with UHPLC−MS/MS and Fluorescence

Marta Sevieri, Cristina Sottani, Arianna Chesi, Arianna Bonizzi, Leopoldo Sitia, Francesco Saverio Robustelli Della Cuna, Elena Grignani, Fabio Corsi,* and Serena Mazzucchelli*

Cite This: https://doi.org/10.1021/acsomega.3c05566

Read Online

ACCESS | Metrics & More | Article Recommendations | Supporting Information

ABSTRACT: We investigated the relevance of encapsulation in H-ferritin nanocages (HFn) in determining an improved tumor-targeted delivery of indocyanine green (ICG). Since from previous experiments, the administration of HFn loaded with ICG (HFn-ICG) resulted in an increased fluorescence signal of ICG, our aim was to uncover if the nanoformulation could have a major role in driving a specific targeting of the dye to the tumor or rather a protective action on ICG's fluorescence. Here, we took advantage of a combined analysis involving ultrahigh performance liquid chromatography−tandem mass spectrometry (UHPLC−MS/MS) on murine tissue homogenates matched with fluorescence intensities analysis detected by ex vivo optical imaging. The quantification of ICG content performed on different organs over time combined with the fluorescent signal detection confirmed the superior delivery of ICG thanks to the nanoformulation. Our results showed that HFn-ICG drives a real accumulation at the tumor instead of only having a role in the preservation of ICG's fluorescence, further supporting its use as a delivery system of ICG for fluorescence-guided surgery applications in oncology.

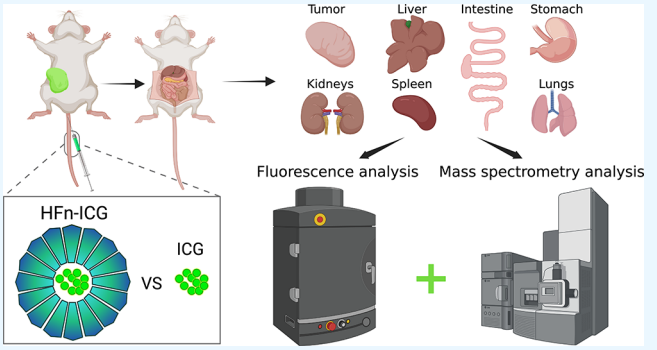

INTRODUCTION

Indocyanine green (ICG) is a safe, water-soluble organic near-infrared (NIR) fluorescent agent introduced as a medical diagnostic tool for NIR fluorescence imaging, since its approval for clinical use in 1959.[1] Following intravenous administration, ICG interacts with plasma proteins and acts as a vascular agent allowing tissue perfusion and lymphatic drainage assessments.[2] This fluorophore has been widely exploited in clinics for angiography and in various surgical fields, including vascular, gastrointestinal, and reconstructive surgery.[3] More recently, ICG has been employed as an optical contrast agent in surgical oncology,[4] and also reported as a photothermal and photosensitizer agent suitable for photothermal and photodynamic therapy in cancer treatment.[2] Despite the excellent biocompatibility and versatility of ICG, its potential application in oncology is strongly limited by its short circulation half-life, aggregation and degradation in aqueous solutions, and lack of tumor specificity.[5]

In this direction, nanotechnology has been widely used for improving ICG's poor stability and in vivo half-life to enhance tumor-specific accumulation by passive or active targeting features displayed by nanoparticles (NPs).[6] Indeed, many advantages stem from the implementation of NPs: (1) the combination or encapsulation of ICG into NPs results in the extension of its half-life; (2) through the functionalization with one or more targeting moieties specific for cancer cells, the selective accumulation of ICG at the tumor site can be achieved; (3) the nanoformulation of ICG may limit its aggregation and photodegradation as well as enhance its stability in aqueous solutions. Starting from this, the development of ICG-based NPs leads the way to several clinical outcomes including, photothermal therapy, photodynamic therapy, and imaging for cancer treatment.[7,8] According to literature, ICG has been loaded or conjugated to a plethora of NPs including lipid-based, polymeric-based,[9,10] and protein-based NPs.[11] Very often these NPs have been further enriched by conjugation with other molecules such as monoclonal antibodies to maximize the specific tumor targeting and employed for cancer theranostic purposes.[11]

Recently, we have proposed the use of H-ferritin nanocages (HFn) as delivery systems of ICG for fluorescence image-guided surgery applications in oncology.[12,13] HFn stands out

Received: July 30, 2023
Revised: October 19, 2023
Accepted: November 22, 2023

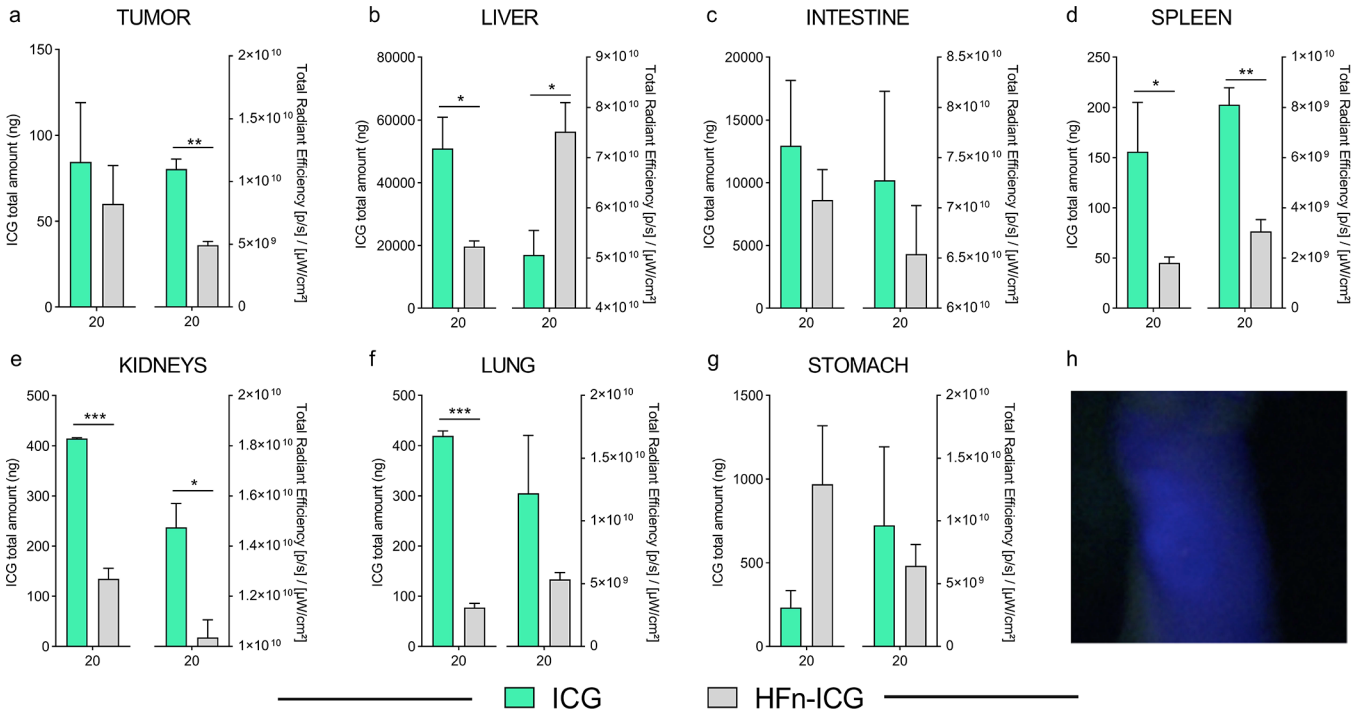

Figure 1. Comparison between ICG concentration measured by UHPLC-MS/MS as ICG total amount and fluorescence detected as total radiant efficiency in tumor (a), liver (b), intestine (c), kidneys (d), spleen (e), lungs (f), and stomach (g) homogenates obtained from mice organs 20 min after injection with ICG or HFn-ICG. Student *t* test * $0.01 < p < 0.02$, ** $0.001 < p < 0.003$, ***$0.00005 < p < 0.0009$. (h) Representative image of mouse injected with HFn-ICG and analyzed after 20 min by KARL STORZ NIR/ICG endoscopic system.

among other nanocarriers by virtue of their capability to specifically target cancer tissues and reduce side effects with a high clinical translational potential and a strong impact in many biomedical applications related to cancer treatment and image-guided surgery.[14] Indeed, it is common knowledge that HFn binds to human cells via interacting with the transferrin receptor 1 (TfR1), which is highly expressed in human cancer cells, therefore being effective as a tumor-targeted delivery vector.[15−17]

Previous studies in which HFn nanocages were loaded with ICG (HFn-ICG) demonstrated their suitability as nanotracers for the identification of the primary tumor mass in comparison to the free dye.[12] Indeed, in vivo experiments already conducted with HFn-ICG confirmed the relevance of the encapsulation in HFn in determining an improved tumor-targeted delivery of ICG.[12] However, the role of HFn encapsulation in determining an improved tumor accumulation of ICG deserves further investigation. In fact, very often, monitoring fluorescence as the only parameter may introduce some bias for an accurate quantification of the molecule in the tissues.[18]

Here, we intend to decipher if the positive impact of the nanoformulation on tumor accumulation of ICG is assured by the more efficient delivery of ICG or is due to a stabilization of its fluorescence.

RESULTS AND DISCUSSION

We have matched and compared the previously obtained ex vivo measurements of fluorescence signal from excised organs,[12] with mass spectrometry analysis performed on the same samples to quantify ICG's content. Our aim was to better understand the dynamics that determined the already observed improved tumor-targeted delivery of ICG with HFn-ICG which resulted in increased visualization of the tumor mass.[12] Indeed, in the present study, we have included in the analyses organs collected from 4T1-tumor bearing BALB/c mice that were randomly divided in two groups, intravenously injected with ICG or HFn-ICG at a concentration of 3.8 mg/kg and killed at different time points (20 min, 1 h, 2 h, 6 h, 24 h, 48 h, 72 h). According to our interpretation, if the improved fluorescence accumulation in tumors is ensured by a better delivery of ICG provided by the nanoformulation, then the profiles achieved by fluorescence and mass spectrometry analyses should be similar. In this way, we will understand if the contribution of HFn encapsulation is solely determined by the stabilization of ICG's fluorescence properties and minimization of its degradation or rather to a specific accumulation. For this purpose, we took advantage of a reliable ultra-high-performance liquid chromatography−tandem mass spectrometer (UHPLC−MS/MS) method for the determination of ICG's content recently developed and validated on liver samples.[19] In compliance with the reduction principle for animal welfare, this approach was also applied to the analysis of organ homogenates obtained from another study, performed in the same experimental conditions.[12]

Results obtained by UHPLC-MS/MS quantification on tumor homogenates were compared with data collected from the ex vivo measurement of fluorescence detected by IVIS Lumina II. After 20 min from the injection, we observed a higher ICG amount measured by UHPLC−MS/MS in most of the organs collected from mice injected with ICG free in comparison to those treated with the same amount of nanoformulated ICG (Figure 1a−g). This quantification reflects the fluorescent levels observed by optical imaging and strongly highlights the nonspecific and widespread behavior of ICG. Indeed, 20 min after intravenous (i.v.)

https://doi.org/10.1021/acsomega.3c05566
ACS Omega XXXX, XXX, XXX−XXX

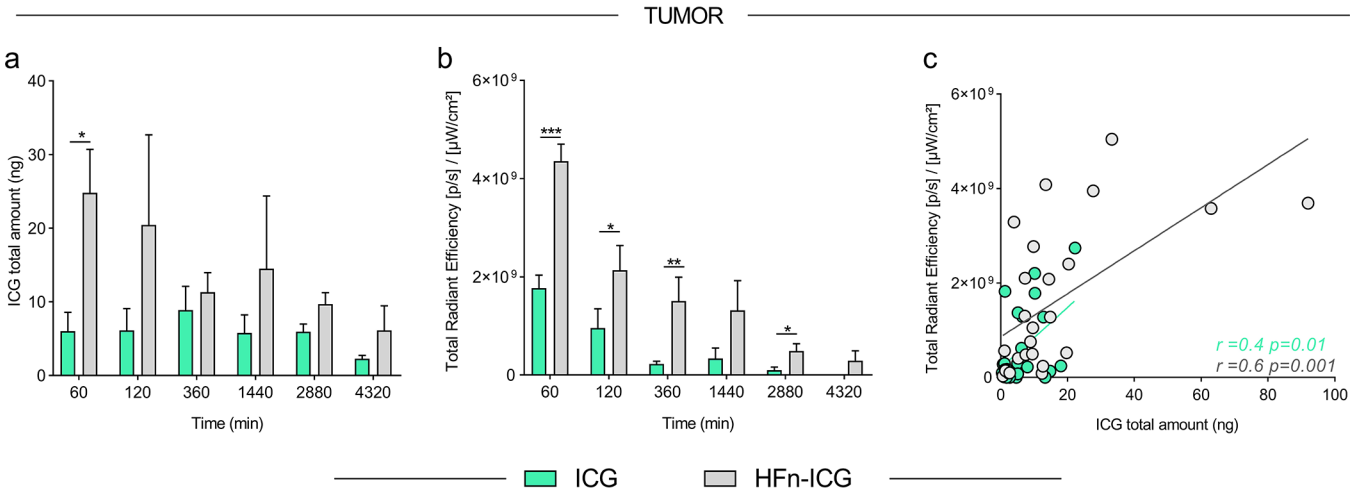

Figure 2. Comparison between ICG concentration measured in tumor homogenates by UHPLC-MS/MS and fluorescence detected at the tumor of mice injected with ICG or HFn-ICG during the biodistribution study (60, 120, 360, 1400, 2880, 4320 min). (a) Bar chart showing the total amount of ICG (ng) measured in tumor homogenates; (b) total fluorescence values detected in tumors. Student t test * $0.02 < p < 0.04$, **$p = 0.004$; ***$p = 0.001$; (c) Scatter plots of the correlation coefficient between the total amount of ICG and total fluorescence detected at the tumor for ICG ($r = 0.4$, $p = 0.01$) and for HFn-ICG ($r = 0.6$, $p = 0.001$).

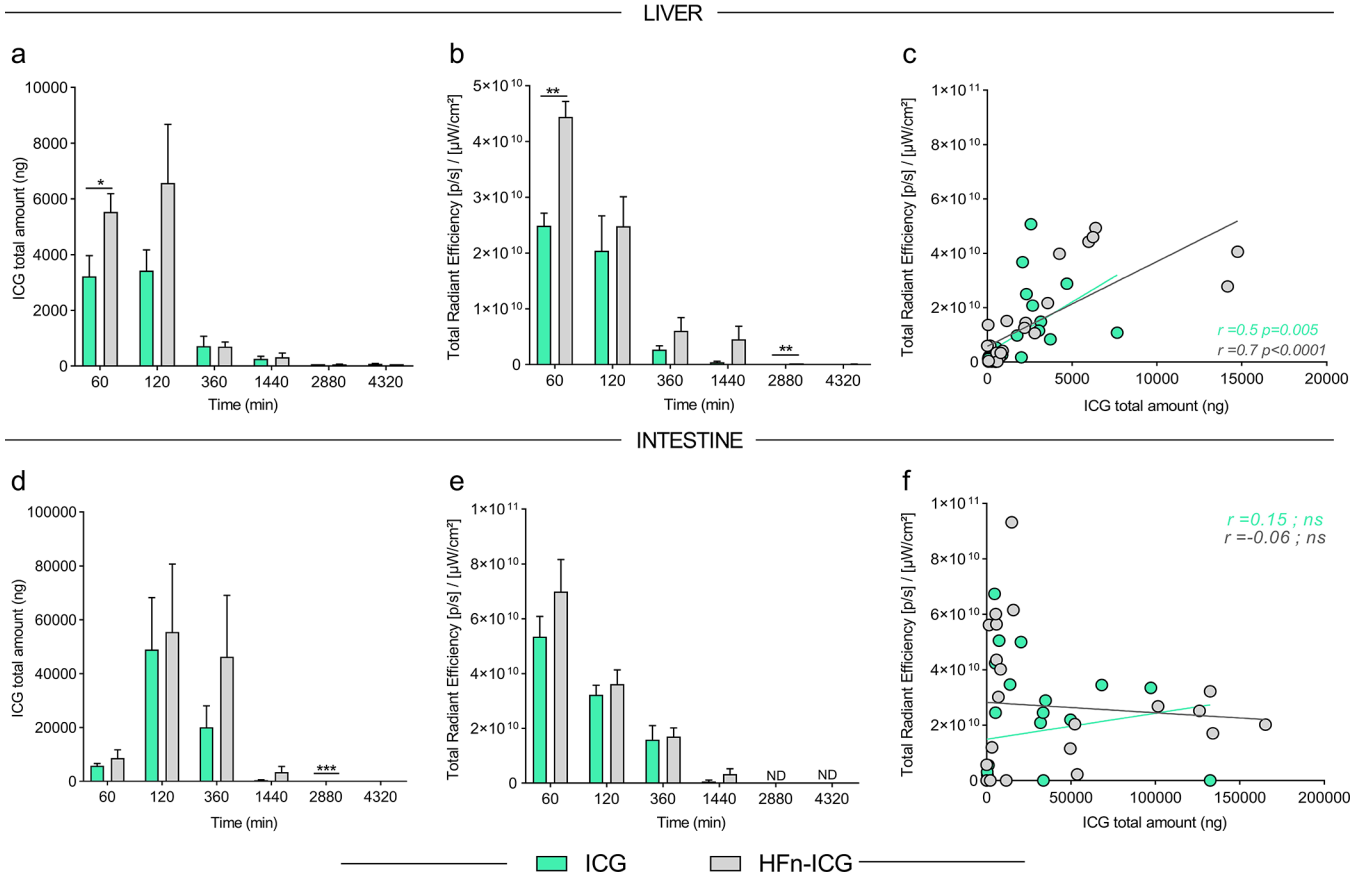

Figure 3. Comparison between ICG concentration measured in liver and intestine homogenates by UHPLC-MS/MS and fluorescence detected at the tumor of mice injected with ICG or HFn-ICG during the biodistribution study (60, 120, 360, 1400, 2880, 4320 min). (a, d) Bar chart showing the total amount of ICG (ng) measured in liver and intestine homogenates. Student t test *$p = 0.04$; ***$p = 0.0007$; (b, e) total fluorescence values detected in liver and intestine. Student t test **$p = 0.002$; (c, f) Scatter plots of the correlation coefficient (r) between the total amount of ICG and total fluorescence detected at liver for ICG ($r = 0.5$, $p = 0.005$) and for HFn-ICG ($r = 0.7$, $p < 0.0001$) and at intestine for ICG ($r = 0.15$, ns) and for HFn-ICG ($r = -0.06$, ns).

administration, ICG spreads faster and permeates the tissues in a nonspecific way. Conversely, ICG nanoformulated in HFn seems to require more time to permeate tissues as a result of a targeted internalization process. The sole exceptions involved the liver in which we observed a higher fluorescent signal associated with the nanoformulation, and the stomach, where

https://doi.org/10.1021/acsomega.3c05566
ACS Omega XXXX, XXX, XXX−XXX

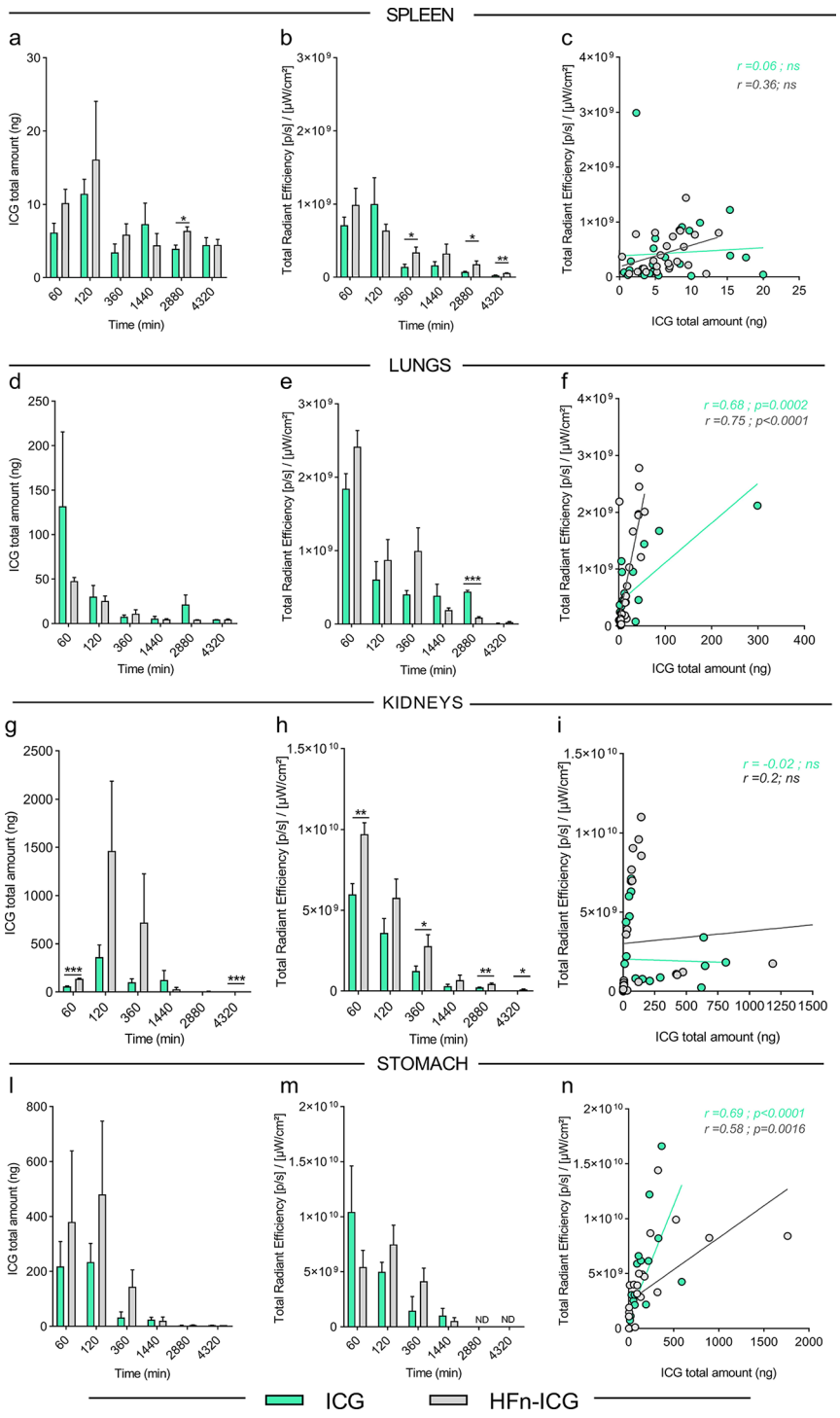

Figure 4. Comparison between ICG concentration measured in spleen, lungs, kidneys, and stomach homogenates by UHPLC-MS/MS and fluorescence detected of mice injected with ICG or HFn-ICG during the biodistribution study. (a) Bar chart showing the total amount of ICG (ng) measured in spleen homogenates; (b) total fluorescence values detected in the spleen; (c) scatter plots of the correlation coefficient between the total amount of ICG and total fluorescence detected at the spleen for ICG (r = 0.06) and for HFn-ICG (r = 0.3). Student t test: * 0.01 < p < 0.04, **p = 0.028. (d) Bar chart showing the total amount of ICG (ng) measured in lungs homogenates; (e) total fluorescence values detected in lungs; (f) scatter plots of the correlation coefficient between the total amount of ICG and total fluorescence detected in the lungs for ICG (r = 0.6, p = 0.0002) and for HFn-ICG (r = 0.7, p < 0.0001). Student t test: ***p = 0.005. (g) bar chart showing the total amount of ICG (ng) measured in kidneys homogenates; (h) total fluorescence values detected in kidneys; (i) Scatter plots of the correlation coefficient between the total amount of ICG and total fluorescence detected at the kidneys for ICG (r = −0.02, ns) and for HFn-ICG (r = 0.2, ns). Student t test: *0.01< p < 0.04; **p = 0.008; ***p = 0.0002; (l) bar chart showing the total amount of ICG (ng) measured in stomach homogenates; (m) total fluorescence values detected in stomach; (n) scatter plots of the correlation coefficient between the total amount of ICG and total fluorescence detected at the stomach for ICG (r = 0.69, p < 0.0001) and for HFn-ICG (r = 0.58, p = 0.0016).

https://doi.org/10.1021/acsomega.3c05566
ACS Omega XXXX, XXX, XXX−XXX

an increased amount of ICG was detected by mass spectrometry, although not statistically significant. A possible explanation for these discrepancies may be associated with the low pH of the gastric environment as well as with a fluorescence quenching effect. However, in order to compare more accurately the signals reported by UHPLC-MS/MS quantifications and ex vivo fluorescence, it was necessary to refer to a specific accumulation of the dye performing the analyses at longer time points. As can be observed in Figure 1h showing the abdominal region of a mouse 20 min after injection of HFn-ICG and analyzed by KARL STORZ NIR/ICG endoscopic system, the fluorescence signal distinguishable in blue is abundantly spread in all districts. Very similar results were observed in mice injected with ICG and imaged 20 min after administration, where any specific accumulation was detected (data not shown).

Afterward, we focused on the accumulation of ICG at the tumor over time to understand to what extent the encapsulation in HFn nanocages drives a specific accumulation of ICG. As shown in Figure 2a, UHPLC-MS/MS quantification on tumor homogenates displays a higher ICG amount at each tested time point in mice injected with HFn-ICG. A similar trend can be observed in relation to the higher levels of fluorescence signal detected in samples obtained from mice injected with HFn-ICG, where a significant difference between the two groups was determined at 1, 2, and 6 h (Figure 2b), confirming the positive contribution of formulation in increased tumor accumulation. Indeed, the higher visualization of the tumor in terms of fluorescent signal is not only due to a protective and stabilizing effect on the fluorescence given by the nanoformulation but also mainly attributable to a specific tumor-targeted delivery. The good correlation (r = 0.6) between the ICG total amount detected by UHPLC-MS/MS quantification and the corresponding fluorescence signal for HFn-ICG and ICG (Figure 1c) confirmed this hypothesis. By contrast, a weaker correlation (r = 4) was determined in samples from mice injected with ICG, evidencing that also a weak ICG stabilizing contribution of HFn nanoformulation may occur. However, the superior tumor accumulation in mice treated with HFn-ICG confirmed its major role in driving ICG tumor homing rather than in the preservation of its fluorescence properties.

Then, we evaluated the biodistribution of ICG both in free form or nanoformulated in the organs involved in ICG metabolism, i.e. liver and intestine. Indeed, it is well-known that ICG is metabolized in the liver, where it is accumulated into bile salts and subsequently released in the intestine and excreted with feces. Figure 3 shows the comparisons between UHPLC-MS/MS results and the evaluations of the fluorescence obtained from homogenates of the liver and intestine. Both considering the accumulation of ICG detected by mass spectrometry (Figure 3a) and fluorescence (Figure 3b) at the liver, no differences were observed. Indeed, the profiles are very similar, as underlined by the good correlation between the ICG total amount detected by UHPLC-MS/MS quantification and the corresponding fluorescence signal for HFn-ICG and ICG (Figure 2c). These results indicate that the encapsulation in HFn does not massively alter the metabolism of ICG, but rather acts by enabling the delivery of a certain amount of ICG to the tumor. Equally, at the other organ involved in ICG metabolism, that is, the intestine, the profiles observed by mass spectrometry and fluorescence signals are substantially comparable (Figure 3e,f). Considering the correlation analysis associated with the liver, a strong correlation was found for HFn-ICG (r = 0.7), while a moderate correlation (r = 0.5) was revealed in mice treated with ICG, suggesting an improved uptake and accumulation in the group injected with HFn-ICG. Otherwise, the analysis performed on intestine samples did not show any correlation between fluorescence and mass results both in HFn-ICG and ICG groups. This could be due to the intestine post mortem cleanup processing during organs harvesting. Indeed, since the complete cleaning and elimination of the stool and food residues are possible only to some extent, it generates some variability that strongly affects the data statistical significance. Moreover, it is worth noticing that the total ICG amount in the tumor is lower than that measured in the liver and intestine. This result is expected since previously published biodistribution studies performed on void HFn evidenced a higher accumulation in the liver in comparison to that observed in the tumor, although they reported that the amount of the drug loaded into ferritin and able to reach the tumor is very effective. Nonetheless, according to our previous results,[20] and other evidence in the literature,[21,22] the preferential accumulation in the liver and kidneys does not prevent a beneficial effect on the tumor. Similarly, we expect that the majority of intravenously administered HFn-ICG as well as ICG, will be sequestered by the liver, metabolized through the hepatobiliary system, released in the intestine as biliary salts, and excreted through feces.

Afterward, we proceeded with the evaluations on homogenates obtained from off-target organs (i.e., spleen, lungs, kidneys, and stomach). In Figure 4a−c, the quantification of ICG is determined in the spleen with the correlated fluorescence quantification. The spleen, both from ICG and HFn-ICG-treated mice, exhibited overall a similar profile in which higher accumulation of HFn-ICG was detected starting from 6 h. With regard to the lungs, as reported in Figure 4d−f, a similar decay was observed, also confirmed by the correlation analysis in Figure 4f. Both the spleen and the lungs displayed low levels of ICG corresponding to low levels of fluorescence starting over the last time points from 6 h after injection, with an order of magnitude of 10^8−10^9. We also investigated the accumulation of ICG in kidneys, which are responsible for HFn clearance. Of note, we observed a high accumulation of HFn-ICG content between 2 and 6 h (Figure 4g), apparently discrepant with detected fluorescence intensities (Figure 4g−i). According to our interpretation, in that time window, HFn-ICG nanocages that reach the kidneys may have already been passed and hence metabolized through the liver. Thus, subsequent to biliary ICG excretion from the liver, the fluorescence properties of ICG could be altered and therefore not detected in the kidneys.

By contrast, the results observed at the stomach (Figure 4l−n) revealed high signals both concerning the concentration determined by mass spectrometry and the fluorescence quantification reaching levels up to an order of magnitude of 10^9−10^{10} (Figure 4m). This outcome was somehow expected considering the results previously obtained.[12] Indeed, despite ICG presence in the stomach being somehow unintended as a consequence of intravenous administration, it is necessary to consider what can happen during the sacrifice. According to our hypothesis, during sacrifice, part of the content of the intestine overflows into the stomach because of the relaxation of the sphincters, as already observed. This leads to the detection of ICG in the stomach, generating a bias that we

https://doi.org/10.1021/acsomega.3c05566
ACS Omega XXXX, XXX, XXX−XXX

cannot overcome. Hence, future in vivo studies will be carried out with a different method of sacrifice to avoid this event.

The aim of this study was to decipher the role of HFn nanocages in improving tumor-targeted delivery of ICG. Indeed, after proving the increased fluorescence signal observed at the tumor mass in mice injected with HFn-ICG, further studies to elucidate the contribution of the nanoformulation become necessary. A validated mass spectrometry method was used to determine the concentrations of ICG in murine organ homogenates. This, coupled with the quantification of fluorescent signal obtained by ex vivo optical imaging, allowed us to depict a reliable scenario of the contribution of nanoformulated ICG in vivo in comparison with ICG free.

The obtained results overall confirmed the relevance of the HFn nanoformulation in driving real accumulation at the tumor. Indeed, after excluding the first time point (i.e., 20 min) to observe a specific accumulation of the dye, the higher fluorescence signal observed at the tumor is associated with a higher amount of ICG in mice injected with HFn-ICG. This also evidenced that the lower accumulation detected in tumors injected with ICG can not only be attributable to a considerable degradation of ICG free but rather to the absence of a specific targeting offered by the encapsulation in ferritin nanocages. Also, by calculating the variation with respect to the first point to study the decrease of the signal, we observed a decay over time for both mass spectrometry and fluorescence determinations, further demonstrating a limited contribution of the nanoformulation in the preservation of the fluorescent signal maintenance (Figure S1, Supporting Information). In addition, our results confirmed that HFn-ICG does not alter the biodistribution of ICG in the organs responsible for its metabolism or in off-target organs. To the best of our knowledge, this is the first time that UHPLC−MS/MS has been used to determine HFn-ICG levels in murine homogenate tissues in a comparative and matched study with fluorescence intensities detected in the same samples. In conclusion, this approach offers a method of particular interest for studying the tissue distribution of ICG and further validates the advantage of nanoformulation in guiding the specific delivery of ICG at the tumor.

■ ASSOCIATED CONTENT

Supporting Information

The Supporting Information is available free of charge at https://pubs.acs.org/doi/10.1021/acsomega.3c05566.

Abbreviation list; materials and methods section; and ICG decay over time observed in mass spectrometry and fluorescence analysis (PDF)

■ AUTHOR INFORMATION

Corresponding Authors

Fabio Corsi − *Nanomedicine Laboratory, Dipartimento di Scienze Biomediche e Cliniche, Università di Milano, Milan 20157, Italy; Breast Unit, Istituti Clinici Scientifici Maugeri IRCCS, Pavia 27100, Italy*; Email: fabio.corsi@unimi.it

Serena Mazzucchelli − *Nanomedicine Laboratory, Dipartimento di Scienze Biomediche e Cliniche, Università di Milano, Milan 20157, Italy*; orcid.org/0000-0001-6904-8895; Email: serena.mazzucchelli@unimi.it

Authors

Marta Sevieri − *Nanomedicine Laboratory, Dipartimento di Scienze Biomediche e Cliniche, Università di Milano, Milan 20157, Italy*

Cristina Sottani − *Environmental Research Center, Istituti Clinici Scientifici Maugeri IRCCS, Pavia 27100, Italy*

Arianna Chesi − *Nanomedicine Laboratory, Dipartimento di Scienze Biomediche e Cliniche, Università di Milano, Milan 20157, Italy*

Arianna Bonizzi − *Nanomedicine Laboratory, Dipartimento di Scienze Biomediche e Cliniche, Università di Milano, Milan 20157, Italy; Breast Unit, Istituti Clinici Scientifici Maugeri IRCCS, Pavia 27100, Italy*

Leopoldo Sitia − *Nanomedicine Laboratory, Dipartimento di Scienze Biomediche e Cliniche, Università di Milano, Milan 20157, Italy*

Francesco Saverio Robustelli Della Cuna − *Environmental Research Center, Istituti Clinici Scientifici Maugeri IRCCS, Pavia 27100, Italy*

Elena Grignani − *Environmental Research Center, Istituti Clinici Scientifici Maugeri IRCCS, Pavia 27100, Italy*

Complete contact information is available at: https://pubs.acs.org/10.1021/acsomega.3c05566

Author Contributions

M.S., A.C., A.B., L.S., F.S.R.C., C.S., and S.M. performed all experiments. Writing and original draft preparation: M.S., C.S., and S.M.; writing—review and editing: E.G., M.S., F.C., and S.M. All authors have read and agreed to the published version of the manuscript.

Notes

The authors declare no competing financial interest.

■ ACKNOWLEDGMENTS

The research leading to these results has received funding from AIRC under IG2022-ID27107 P.I. Mazzucchelli and from the University of Milan (Linea 2). We acknowledge the University of Milan for M. S. PhD fellowship, and AIRC IG2022-ID27107 P.I. Mazzucchelli for L.S. postdoctoral position. The authors acknowledge the University of Milan for support in open access publication.

■ REFERENCES

(1) Lu, C.-H.; Hsiao, J.-K. Indocyanine Green: An Old Drug with Novel Applications. *Tzu Chi Med J* **2021**, *33* (4), 317.

(2) Sheng, Z.; Hu, D.; Xue, M.; He, M.; Gong, P.; Cai, L. Indocyanine Green Nanoparticles for Theranostic Applications. *Nano-Micro Lett.* **2013**, *5* (3), 145−150.

(3) Leiloglou, M.; Kedrzycki, M. S.; Chalau, V.; Chiarini, N.; Thiruchelvam, P. T. R.; Hadjiminas, D. J.; Hogben, K. R.; Rashid, F.; Ramakrishnan, R.; Darzi, A. W.; Leff, D. R.; Elson, D. S. Indocyanine Green Fluorescence Image Processing Techniques for Breast Cancer Macroscopic Demarcation. *Sci Rep* **2022**, *12* (1), 8607.

(4) Alam, I. S.; Steinberg, I.; Vermesh, O.; Van Den Berg, N. S.; Rosenthal, E. L.; Van Dam, G. M.; Ntziachristos, V.; Gambhir, S. S.; Hernot, S.; Rogalla, S. Emerging Intraoperative Imaging Modalities to Improve Surgical Precision. *Mol Imaging Biol* **2018**, *20* (5), 705−715.

(5) Fernandez-Fernandez, A.; Manchanda, R.; Lei, T.; Carvajal, D. A.; Tang, Y.; Kazmi, S. Z. R.; McGoron, A. J. Comparative Study of the Optical and Heat Generation Properties of IR820 and Indocyanine Green. *Mol. Imaging* **2012**, *11* (2), 99−113.

(6) Sevieri, M.; Silva, F.; Bonizzi, A.; Sitia, L.; Truffi, M.; Mazzucchelli, S.; Corsi, F. Indocyanine Green Nanoparticles: Are They Compelling for Cancer Treatment? *Front. Chem.* **2020**, *8*, 535.

(7) Hill, T. K.; Abdulahad, A.; Kelkar, S. S.; Marini, F. C.; Long, T. E.; Provenzale, J. M.; Mohs, A. M. Indocyanine Green-Loaded Nanoparticles for Image-Guided Tumor Surgery. *Bioconjugate Chem.* **2015**, *26* (2), 294−303.
(8) Bortot, B.; Mangogna, A.; Di Lorenzo, G.; Stabile, G.; Ricci, G.; Biffi, S. Image-Guided Cancer Surgery: A Narrative Review on Imaging Modalities and Emerging Nanotechnology Strategies. *J Nanobiotechnol* **2023**, *21* (1), 155.
(9) Wang, H.; Li, X.; Tse, B. W.-C.; Yang, H.; Thorling, C. A.; Liu, Y.; Touraud, M.; Chouane, J. B.; Liu, X.; Roberts, M. S.; Liang, X. Indocyanine Green-Incorporating Nanoparticles for Cancer Theranostics. *Theranostics* **2018**, *8* (5), 1227−1242.
(10) Ting, C.-W.; Chou, Y.-H.; Huang, S.-Y.; Chiang, W.-H. Indocyanine Green-Carrying Polymeric Nanoparticles with Acid-Triggered Detachable PEG Coating and Drug Release for Boosting Cancer Photothermal Therapy. *Colloids and Surfaces B: Biointerfaces* **2021**, *208*, No. 112048.
(11) Gowsalya, K.; Yasothamani, V.; Vivek, R. Emerging Indocyanine Green-Integrated Nanocarriers for Multimodal Cancer Therapy: A Review. *Nanoscale Adv.* **2021**, *3* (12), 3332−3352.
(12) Sevieri, M.; Sitia, L.; Bonizzi, A.; Truffi, M.; Mazzucchelli, S.; Corsi, F. Tumor Accumulation and Off-Target Biodistribution of an Indocyanine-Green Fluorescent Nanotracer: An Ex Vivo Study on an Orthotopic Murine Model of Breast Cancer. *IJMS* **2021**, *22* (4), 1601.
(13) Sitia, L.; Sevieri, M.; Bonizzi, A.; Allevi, R.; Morasso, C.; Foschi, D.; Corsi, F.; Mazzucchelli, S. Development of Tumor-Targeted Indocyanine Green-Loaded Ferritin Nanoparticles for Intraoperative Detection of Cancers. *ACS Omega* **2020**, *5* (21), 12035−12045.
(14) Mainini, F.; Bonizzi, A.; Sevieri, M.; Sitia, L.; Truffi, M.; Corsi, F.; Mazzucchelli, S. Protein-Based Nanoparticles for the Imaging and Treatment of Solid Tumors: The Case of Ferritin Nanocages, a Narrative Review. *Pharmaceutics* **2021**, *13* (12), 2000.
(15) Fan, K.; Cao, C.; Pan, Y.; Lu, D.; Yang, D.; Feng, J.; Song, L.; Liang, M.; Yan, X. Magnetoferritin Nanoparticles for Targeting and Visualizing Tumour Tissues. *Nature Nanotech* **2012**, *7* (7), 459−464.
(16) Truffi, M.; Fiandra, L.; Sorrentino, L.; Monieri, M.; Corsi, F.; Mazzucchelli, S. Ferritin Nanocages: A Biological Platform for Drug Delivery, Imaging and Theranostics in Cancer. *Pharmacol. Res.* **2016**, *107*, 57−65.
(17) Chen, Y.; Zeng, L.; Zhu, H.; Wu, Q.; Liu, R.; Liang, Q.; Chen, B.; Dai, H.; Tang, K.; Liao, C.; Huang, Y.; Yan, X.; Fan, K.; Du, J.; Lin, R.; Wang, J. Ferritin Nanocaged Doxorubicin Potentiates Chemo-Immunotherapy against Hepatocellular Carcinoma via Immunogenic Cell Death. *Small Methods* **2023**, *7* (5), No. 2201086.
(18) Hardy, N. P.; MacAonghusa, P.; Dalli, J.; Gallagher, G.; Epperlein, J. P.; Shields, C.; Mulsow, J.; Rogers, A. C.; Brannigan, A. E.; Conneely, J. B.; Neary, P. M.; Cahill, R. A. Clinical Application of Machine Learning and Computer Vision to Indocyanine Green Quantification for Dynamic Intraoperative Tissue Characterisation: How to Do It. *Surg Endosc* **2023**, *37* (8), 6361−6370.
(19) Sottani, C.; Grignani, E.; Cottica, D.; Mazzucchelli, S.; Sevieri, M.; Chesi, A.; Corsi, F.; Galfrè, S.; Robustelli Della Cuna, F. S.; Calleri, E Development and Validation of a Bioanalytical UHPLC-MS/MS Method Applied to Murine Liver Tissue for the Determination of Indocyanine Green Loaded in H-Ferritin Nanoparticles. *Front. Chem.* **2022**, *9*, No. 784123.
(20) Mazzucchelli, S.; Bellini, M.; Fiandra, L.; Truffi, M.; Rizzuto, M. A.; Sorrentino, L.; Longhi, E.; Nebuloni, M.; Prosperi, D.; Corsi, F. Nanometronomic Treatment of 4T1 Breast Cancer with Nanocaged Doxorubicin Prevents Drug Resistance and Circumvents Cardiotoxicity. *Oncotarget* **2017**, *8* (5), 8383−8396.
(21) Zhang, Y.-N.; Poon, W.; Tavares, A. J.; McGilvray, I. D.; Chan, W. C. W. Nanoparticle−Liver Interactions: Cellular Uptake and Hepatobiliary Elimination. *J. Controlled Release* **2016**, *240*, 332−348.
(22) Reinhart, M. B.; Huntington, C. R.; Blair, L. J.; Heniford, B. T.; Augenstein, V. A. Indocyanine Green: Historical Context, Current Applications, and Future Considerations. *Surg Innov* **2016**, *23* (2), 166−175.

https://doi.org/10.1021/acsomega.3c05566
ACS Omega XXXX, XXX, XXX−XXX